Identification of optimum operatives parameters for Pulse Nd:YAG laser in paint removal on different types of car coated substrate

***Mohammad Khairul Azhar Abdul Razab[1,2], Mohamad Suhaimi Jaafar[2], Azhar Abdul Rahman[2] and Syahrul Affandi Saidi[2]**

1. *Faculty of Earth Sciences, Universiti Malaysia Kelantan Jeli Campus, Locked Bag No. 100, 17600 Jeli, Kelantan, Malaysia.*
2. *School of Physics, Universiti Sains Malaysia Main Campus, 11800 Minden, Penang, Malaysia.*

Abstract

The optimum operatives parameters of Cynosure Cynergy Pulse Nd:YAG laser in paint removal process has been identified on three types of car coated substrate samples A, B and C with the coating thicknesses ranging from 92 – 134 μm, 196 – 450 μm and 219 – 283 μm respectively. Alicona IFM G4 analysis was done on 540 irradiated craters in obtaining the depth thickness (*d*) between the crater surface level and top coating surface level for average coating removal efficiency (ϵ) determination. FESEM and EDX analysis were done to reveal the physical and chemical characteristics of best selected crater depth accounted from the highest ϵ obtained. In this study, the optimum operatives process for sample A is set-up with pulse width (PW) 100 ms, repetition rate (RR) 1.0 Hz and beam size (BS) 5 mm at *F* 180 J/cm^2. The optimum operative process for Sample B is set up with PW 200 ms, RR 1.0 Hz, BS 5 mm at *F* 220 J/cm^2 whereas the optimum operative process for sample C is set-up with PW 100 ms, RR 2.0 Hz, BS 5 mm at *F* 150 J/cm^2.

Keywords: Nd:YAG laser, Laser parameters, Paint removal, Car coated substrate, Crater depth

1. Introduction

Studies shows that laser cleaning can be a good alternative candidate to replace conventional chemical cleaning in paint removal purposes which consume much water and cost, (Chen, Kwee, Tan, Choo, & Hong, 2010; Steen & Mazumder, 2010). This new cleaning methods also has advantages in absence of mechanical damage of the metal surface and at the same time increase the effectiveness of paint removal, (Veiko, Mutin, Smirnov, Shakhno, & Batishche, 2008). The term laser cleaning is related with two quite different areas which are the removal of unwanted layers and another one is the removal of extended contamination of unwanted layers from solid surface, (Bäuerle, 2011). Both different areas include as cleaning solid or metals substrate from foreign organic impurities and removal of existed paint from metal surfaces, (Kane, 2006). Unique characteristics of laser cleaning utilize the versatile, precise, controllable, selective and environmentally friendly process to strip the paint from substrate surfaces in many industries, (Lee & Watkins, 2000).

However, the information of laser cleaning techniques in automotive industry is less discussed as well as their efficiency process and optimum of laser parameters is not well documented. The selection of appropriate laser parameters is vital in laser cleaning process,

(Sanjeevan & Klemm, 2005). Several parameters should be considered during the process are laser wavelength (λ), laser fluence (*F*), beam size (BS), pulse width (PW) and repetition rate (RR), (Brygo et al., 2006). Inappropriate selection of laser parameters lead to overexpose which result in substrate damage due to the high energy density of the laser beam whereas underexpose can leave the residual contamination on the substrate surface, (Lee & Watkins, 2000). Nevertheless, the damage to the substrate material can be eliminated by applying the right operative laser parameters with no outside distraction factors involved during the process, (Heidelmann, 2011). Due to this situation, the optimum operatives process parameters of Cynosure Cynergy Pulse Nd:YAG laser in paint removal will be determined on three selective car coated substrate, hence reduced the risk of metal substrate damage.

2. Experimental

2.1 Substrate samples preparation

In this study, 54 rectangular shapes of car coated substrate samples will prepare consist of car models A, B and C. Each type required 18 samples to be irradiated with ten laser irradiation spotted on each sample, thus 540 irradiations will be done for all three samples A, B and C. Samples A and B are carried out from two types of national car model made in the year of 2008 and 2000 with the coating type of orange metallic acrylic and black metallic acrylic, whereas samples C is carried out from a type of imported car model made in the year of 1992 with the coating type is green solid (non-metallic) acrylic paint. The samples will be cutting in small rectangular substrate, approximately to 4 x 4 cm^2 in size for Alicona Infinite Focus Metrology (IFM) G4, Field Emission Scanning Electron Microscopy (FESEM) and Energy Dispersive X-ray (EDX) analysis availability. The paint thickness determined by using CEM DT-156 Paint Coating Thickness Gauge Tester F/NF Probe for substrate samples A, B and C are ranging from 92 – 134 μm, 196 – 450 μm, 219 – 283 μm respectively and never repaints.

Each substrate sample will be marking by unique number from 1 to 18 at the edge of back side for sample number identification. An each sample will prepared for ten irradiations with increase in their *F* given. Thus, ten dots will marked by using permanent marker pen on the coating surface of a substrate sample, which followed by a series number from one to ten at the backside for irradiation spot identification. Specifically, the series number represents the laser irradiation has been done for a certain dot spot, means the first irradiation is indicating by number 1 and tenth irradiation is indicating by number 10. Irradiation number 1 is set-up for highest *F* whereas irradiation number 10 is set-up for lowest *F*.

2.2 Sample irradiation

For first irradiation, laser parameters are set-up with *F* 300 J/cm^2, PW 100 ms and RR 1.0 Hz. The instruments are ensuring to locate on the right location of experimental set-up as shown in Figure 1. Second and next irradiation will be done on the same sample but on the different dot target by reduce the *F* to 290, 280, 270, 260, 250, 240, 230, 220 and 210 J/cm^2. For this irradiation, the PW and RR will be fixed at 100 ms and 1.0 Hz respectively. The experiments will repeat on the next samples by manipulating the PW and RR as listed in the Table 1. Protective safety eyewear is wearing during the whole experiments in order to protect the eyes from the hazard of laser irradiation.

Each irradiated samples will be cleaned using plain water and dried to remove any burning residue existed after irradiation has been completed. Tissue paper will be using to swap the stripped area in order to ensure there are no more residues of paint flakes left. More important, the originality of the structure, pattern, contour and texture of the irradiated crater depth will be sustaining from any physical and chemical distortion before proceed to IFM G4 analysis.

2.3 Crater depth selection

Alicona IFM G4 is using to analyze 540 irradiated crater depths to obtain the optical surface micrograph and its corresponding profilometer graph. Depth profilometer analysis provides a pattern of graphical illustration between crater surface level and top coating surface level with precise vertical measurement of the crater depth (Alicona, 2011). For this study, depth thickness (*d*) versus *F* graphs is plotting for each PW, RR and BS considered. Hence the average coating removal efficiency (ϵ) of each laser parameters applied on a certain car coated substrate sample will determined by measuring their inclination of each fitted linear graph. Finally, the summarize of ϵ for each three types of substrate samples and their corresponding laser parameters considered will presents in Table 2.

The highest ϵ for sample A, B and C are 1.75 $\mu m\ cm^2\ J^{-1}$, 1.12 $\mu m\ cm^2\ J^{-1}$ and 1.65 $\mu m\ cm^2\ J^{-1}$ respectively. Actually, the highest ϵ for sample B is obtaining at 4.94 $\mu m\ cm^2\ J^{-1}$ from sample B8, but the result produced is considering invalid in term of profilometer depth measurements. To overcomes this doubtful result, the sample B11 will selected as the highest ϵ for sample B at 1.12 $\mu m\ cm^2\ J^{-1}$.

There is an optimum laser parameters in obtaining the best efficiency of laser paint removal based on physical and chemical characteristics of both coating and substrates, (Zhou et al., 2001). For this study, the selection of the best crater depth from the highest ϵ is based on the best evaluation of IFM optical micrograph by naked eyes in term of smoothness of the contour structure obtained, unaffected of surface painted layer around the region of interest (ROI), uniform surface texture and less roughen of the crater depth as represents in Appendix 1 - 3. The best selected crater depth for each substrate sample A, B and C is listed in Table 3.

3. Results and discussions

3.1 IFM results

IFM optical micrograph and their corresponding profilometer for the best selected crater depth as listed in Table 3 will deeply analyzed. Figure 2 and 3 shows the micrograph contour pattern and its corresponding profilometer obtained from sample A10 on crater depth number 7. This selected crater depth is considering the best in term of highest ϵ, smoothness of the contour structure obtained, unaffected of surface painted layer around the ROI, uniform surface texture and less roughen of the crater depth.

Figure 4 and 5 shows the IFM micrograph contour pattern and its corresponding profilometer obtained from sample B11 on crater depth number 3. This type of crater depth considered the best in term of highest ϵ, thin residue of paint flakes around the crater wall obtained and unaffected of painted surface outside the crater depth area.

Meanwhile, the IFM micrograph contour pattern and its corresponding profilometer obtained from sample C16 on crater depth number 1 is shown in Figure 6 and 7. The selected crater

depth considered the best in term of highest result ϵ, less residues of top and base surface layers which unable to remove but able to identify the contour pattern structure obtained.

3.2 FESEM and EDX results

FESEM analysis for surface morphology and EDX analysis for elemental composition represents in term of atomic percentage (at. %) and weight percentage (wt. %) will be investigating on the best selected crater depth as listed in Table 3 by using Nova NanoSEM 450. Moreover, the non-irradiated ROI will select randomly from substrate samples A, B and C for EDX analysis and becomes a control for their corresponding group types as shown in Table 7.

Figure 8 and Table 4 shows the surface morphology and elemental composition obtained from sample A10 on crater depth number 7. From the micrograph, the selected crater depth produced a few of subtle line represents the fine cracks followed by a few of small holes along and nearest to the line. However, the surface morphology is uniform in term of their texture and structure.

Figure 9 and Table 5 shows the surface morphology and elemental composition of sample B11 on a crater depth number 3. The selected crater depth does not produce any subtle or coarse line that represents the fine cracks. However, many of small holes together with their minor grain spherical surface are detected around the ROI. This condition leads to non-uniformity of the crater surface texture and structure.

Figure 10 and Table 6 revealed the surface morphology and elemental composition obtained from sample C16 on a crater depth number 1. The selected crater depth obtained minor grain amorphous surface. In addition, many of small holes detected around the ROI leads to non-uniform of crater surface texture and structure.

3.2 Physical and chemical characteristic of the best crater depth

The profilometer and its optical micrograph gives the information of paint thickness has been removed and uniformity of selected crater surface for sample A, B and C as shown in Figure 2 – 7. From the results, the paint material of sample A and B is considered has been removed uniformly, whereas non-uniform crater surface obtained in sample C indicates the top layer of paint material is still unremoved. It is clearly shown by smooth profilometer and identified of contour pattern of sample A and B in Figure 3 and 5, but conversely happened for sample C where the profilometer produced more unintended peak, unidentified and complex contour pattern as shown in Figure 7.

This might be due to thermal distribution is uniformly distributed onto the crater surface of sample A and B but randomly distributed onto sample C. This factor might be due to the paint material in sample C has lowest diffusivity and unable to distribute the thermal of *F* effectively. This condition results to non-uniform of 'thermal pool' distribution level, hence reduced the thermal decomposition process on the painted material.

However, all optical micrograph has shows the 'wavelike' rings around the edge of the crater due to resolidified of the molten paint material, (Kearns et al., 1998). The 'wavelike' rings are most critical on the sample C, followed by sample A and B as shown in Appendix 1 - 3. This is because the characteristics of paint material itself, where the paint layer onto the sample C and A is more tight to be removed and tend to be melting during the thermal decomposition process.

On the other hand, the 'wavelike' rings pattern obtained around the crater depth is inevitable due to the non-uniform intensity of Gaussian shape laser beam, (Shu-Dong et al., 2012). Due to this,

the concave depth is clearly seen from the optical micrograph and profilometer obtained where the depth is maximum at the central of the irradiated area but minimum at the edge side around the crater depth. This is because the laser concentration is always higher at the centre of beam focal plane, (Bäuerle, 2011).

Properties of the surface morphology are depending on the efficiency of the thermal decomposition process occurred on the paint layer, whether the paint layer has uniformly removed or still left the paint residues after the irradiation process. From the results, a few defects on the crater depth detected for irradiated of sample A, B and C sort of cracking, fine and coarse line obtained, grain spherical surface, amorphous carbon shape of the crater surface and many more. These defects is mainly due to thermal induce resulted from thermal decomposition mechanism during paint removal process, (Chen, et al., 2010; Labuschagne & Pityana, 2005).

Paint removal considered to almost complete for best crater depth selected from the highest ϵ micrograph of sample A as shown in Figure 8 where a few of precipitate subtle line obtained. For sample B, the best crater depth selected from highest ϵ produced minor grain spherical shape and small holes is detected around the surface as shown in Figure 9. This shows that paint material is not uniformly removed where the surface texture is roughening and non-uniform. Same goes to the sample C, the best crater depth selected from highest ϵ obtained the minor epitaxial growth amorphous shape as shown in the Figure 10. For this sample type, the paint residue is considered very thick and non-uniform where the laser *F* only removed a certain location of the paint layers.

All the irradiated samples considered to reveal the pretreatment coating which nearest to the bare metal. This will be proving by the detection of Zn element that recognized as the main element for anticorrosive and at the same time acts to enhance the adhesivity between the paint material to the metal substrate as shown in Table 4 - 6, (Cottam, Emmony, Cuesta, & Bradley, 1998). Other non-metallic elements like O and C which changing in their atomic weight during the stripping process also detected. The decreasing of C and increasing of O elements in sample A and B proved the some part of plasma cleaning occurred via oxidation process as shown in Table 4 and 5, (Cottam, et al., 1998).

Moreover, the paint removal for selected crater depth of samples A and B considered to not reaching the bare metal where the O concentration is still increasing from the original composition as shown in Table 4 and 5 compared to Table 7. It is found that monitoring the oxygen concentration gives a full indication when a bare metal surface is generating, as the removal of the primer coat will decreased the oxygen concentration to a minimum when a bare metal surface is reaching, (Siggs, 2010).

However, the changing of C and O concentration did not give any significant information for sample C due to the top coat to pretreatment layers has been accounted by EDX analysis. This is because the maximum paint removal is considered to be occurring into the small hole at the center of the crater depth, but left a few layers of painted material around the depth to be detected by using EDX analysis.

Conclusion

In this study, the optimum operatives process for sample A is set-up with PW 100 ms, RR 1.0 Hz and BS 5 mm at *F* 180 J/cm^2. On the other hand, the optimum operative process for Sample B is set up with PW 200 ms, RR 1.0 Hz, BS 5 mm at *F* 220 J/cm^2. Meanwhile, the optimum operative process for sample C is set-up with PW 100 ms, RR 2.0 Hz, BS 5 mm at *F* 150 J/cm^2. The thermal effects results considered to did not give any risk to the metal substrate damage since the

bare metal is not directly exposed to the laser *F*. This research study prove the effectiveness, quality and efficiency of paint removal process can be obtained by using Cynosure Cynergy Pulse Nd:YAG laser with optimum selection of laser parameters.

Acknowledgment

The authors acknowledge the support of the Research University-Postgraduate Research Grant Scheme (RU-PRGS) [Grant Number 1001/PFIZIK/845008] awarded by Universiti Sains Malaysia. Great appreciation goes to Ministry of Higher Education and Universiti Malaysia Kelantan for providing a scholarship and financial assistance for this research project. Appreciation also goes to Mr. Mohd Ashamuddin Hashim of the School of Mechanical Engineering and Mrs. Ee Bee Choo of the School of Physics, Universiti Sains Malaysia for their help in Alicona IFM G4, FESEM and EDX analysis.

References

Alicona, I. G. (2011). IFM G4 3.5.1.5 EN 27.04. 2011. *Alicona GmbH*.

Bäuerle, D. (2011). *Laser processing and chemistry*: Springer.

Brygo, F., Dutouquet, C., Le Guern, F., Oltra, R., Semerok, A., & Weulersse, J. (2006). Laser fluence, repetition rate and pulse duration effects on paint ablation. *Applied surface science, 252*(6), 2131-2138.

Chen, G., Kwee, T., Tan, K., Choo, Y., & Hong, M. (2010). Laser cleaning of steel for paint removal. *Applied Physics A, 101*(2), 249-253.

Cottam, C., Emmony, D., Cuesta, A., & Bradley, R. (1998). XPS monitoring of the removal of an aged polymer coating from a metal substrate by TEA-CO2 laser ablation. *Journal of materials science, 33*(13), 3245-3249.

Heidelmann, G. (2011). Surface Cleaning with Laser Technology.

Kane, D. M. (2006). *Laser cleaning II*: World Scientific.

Kearns, A., Fischer, C., Watkins, K., Glasmacher, M., Kheyrandish, H., Brown, A., et al. (1998). Laser removal of oxides from a copper substrate using Q-switched Nd: YAG radiation at 1064 nm, 532 nm and 266 nm. *Applied surface science, 127*, 773-780.

Labuschagne, K., & Pityana, S. (2005). Laser induced damage threshold on metallic surfaces during laser cleaning.

Lee, J., & Watkins, K. (2000). In-process monitoring techniques for laser cleaning. *Optics and lasers in engineering, 34*(4), 429-442.

Sanjeevan, P., & Klemm, A. (2005). *A Review of Laser Technique Application in Cleaning Process of Porous Construction Materials*. Paper presented at the PRoBE Conference.

Shu-Dong, S., Wei, L., Peng, D., Meng, W., Feng, S., Shu-Jing, L., et al. (2012). Removing paint from a metal substrate using a flattened top laser. *Chinese Physics B, 21*(10), 104209.

Siggs, E. B. (2010). *Laser and electron beam treatments for corrosion protection of friction stir welds in aerospace alloys.* Unpublished Ph.D thesis, University of Birmingham.

Steen, W. M., & Mazumder, J. (2010). *Laser material processing*: Springer.

Veiko, V., Mutin, T. J., Smirnov, V., Shakhno, E., & Batishche, S. (2008). *Laser cleaning of metal surfaces: physical processes and applications.* Paper presented at the Fundamentals of Laser Assisted Micro-and Nanotechnologies.

Zhou, X., Imasaki, K., Furukawa, H., Umino, H., Sakagishi, K., Nakai, S., et al. (2001). A study of the surface products on zinc-coated steel during laser ablation cleaning. *Surface and Coatings Technology, 137*(2), 170-174.

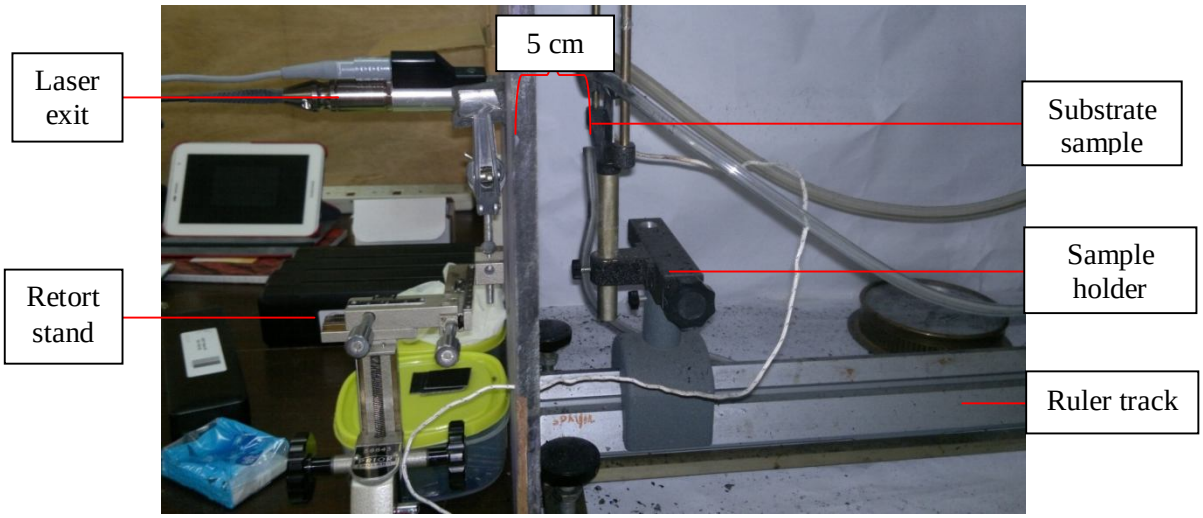

Figure 1: Experimental set-up for laser paint removal on the car coated substrate.

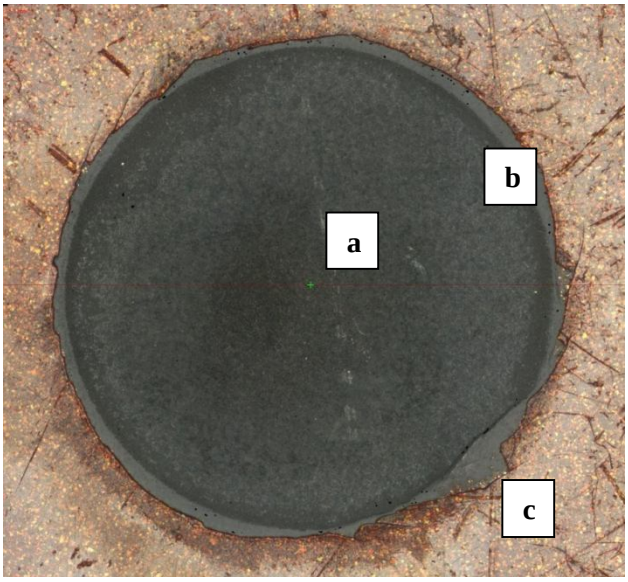

Figure 2: IFM micrograph for PW 100 ms, RR 1.0 Hz, BS 5 mm and fluence energy 180 J/cm2 for sample A10 on crater depth number 7; a. Uniform crater surface obtained, b. Contour is easily identify and obtained in smooth pattern, c. Unaffected of surface painted layer.

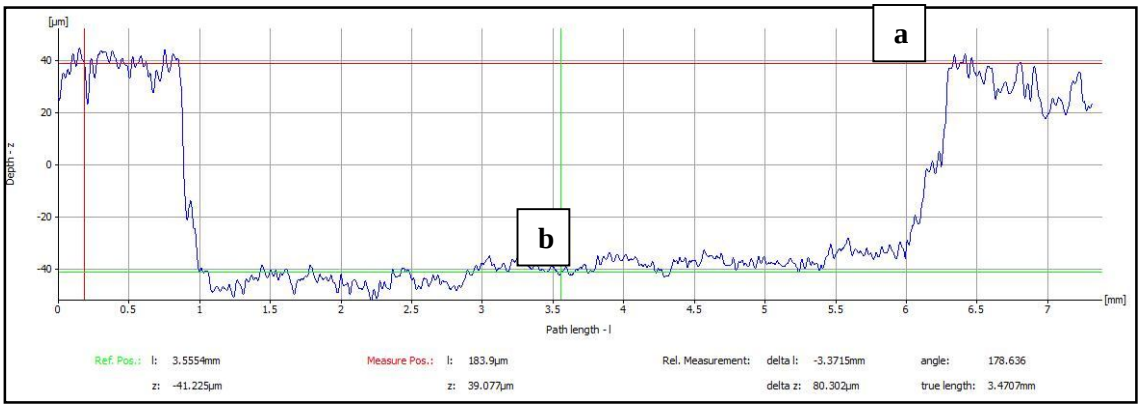

Figure 3: IFM depth profile (*d*) for PW 100 ms, RR 1.0 Hz, BS 5 mm and fluence energy 180 J/cm^2 for sample A10 on crater depth number 7; a. Both side of painted surface is uniform on the reference line (red line) with no peak (identified contour) produced, b. Crater surface texture is more uniform with micro roughness appeared.

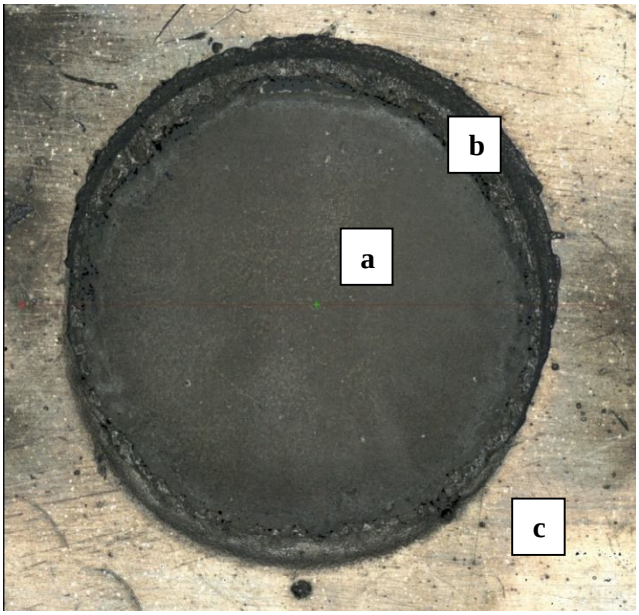

Figure 4: IFM micrograph for PW 200 ms, RR 1.0 Hz, BS 5 mm and fluence energy 220 J/cm^2 for sample B11 on crater depth number 3; a. Uniform surface texture of crater depth, b. Thin residue of paint flake attached around the crater wall, c. Original colour of painted surface unaffected.

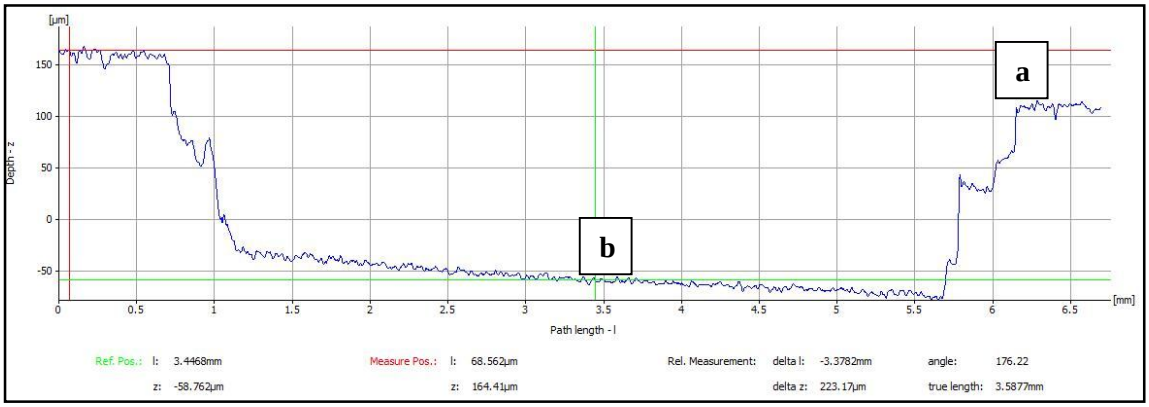

Figure 5: IFM depth profile (*d*) for PW 200 ms, RR 1.0 Hz, BS 5 mm and fluence energy 220 J/cm^2 for sample B11 on crater depth number 3; a. Both side of crater edge is uniform and did not exceed the reference line (red line) and easy to identify the contour pattern, b. Crater surface texture is uniform with micro roughness pattern detected.

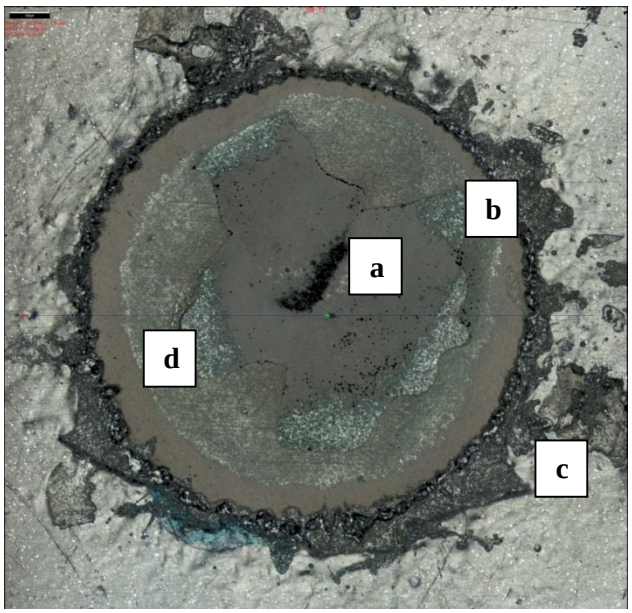

Figure 6: IFM micrograph for PW 100 ms, RR 2.0 Hz, BS 5 mm and fluence energy 150 J/cm^2 for sample C16 on crater depth number 1; a. Uniform surface texture at the center of crater depth, b. Contour is not too smooth but able to identify, c. Effected of surface painted layer, d. Less residues of top and base surface layer which unable to removed.

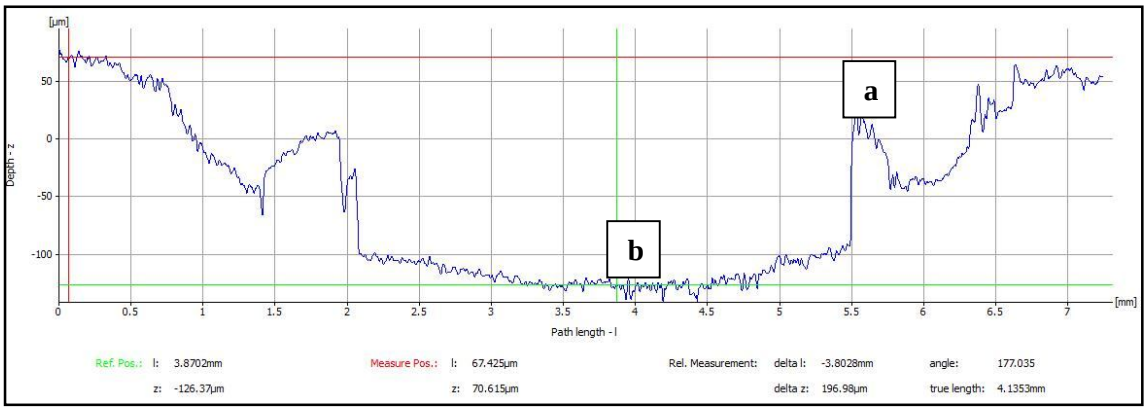

Figure 7: IFM depth profile (*d*) for PW 100 ms, RR 2.0 Hz, BS 5 mm and fluence energy 150 J/cm^2 for sample C16 on crater depth number 1; a. The peak is obtained representing the residue of top and base layer unable to remove as shown in Figure 6 (d), b. Micro roughness pattern and uniform texture is produced at the centre of crater surface.

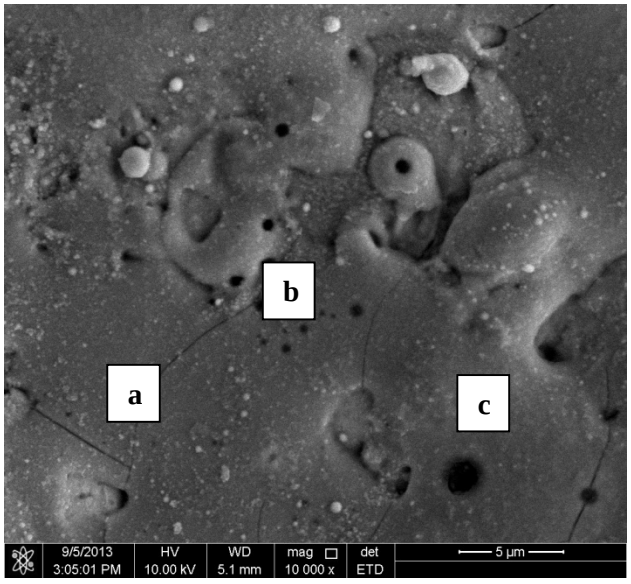

Figure 8: Surface morphology for PW 100 ms, RR 1.0 Hz, BS 5 mm and fluence energy 180 J/cm2 for sample A10; a. Precipitate subtle line obtained on the ROI selected represents the fine cracks on the irradiated surface, b. A few of small holes clearly seen on the crater surface at 10 x 10^3 times image magnification, c. Surface morphology is uniform in term of their texture and structure.

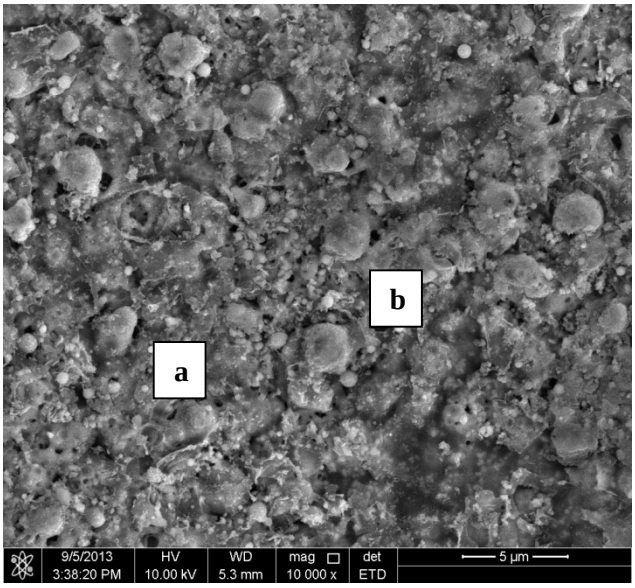

Figure 9: Surface morphology for PW 200 ms, RR 1.0 Hz, BS 5 mm and fluence energy 220 J/cm^2 for sample B11; a. Minor grain spherical shape clearly seen on the ROI selected, b. Many of small holes detected around the irradiated surface.

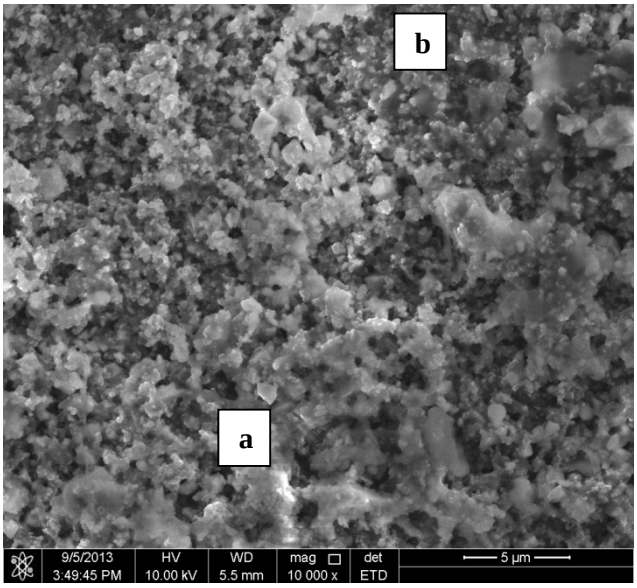

Figure 10: Surface morphology for PW 100 ms, RR 2.0 Hz, BS 5 mm and fluence energy 150 J/cm^2 for sample C16; a. Minor epitaxial growth in amorphous shape clearly seen on the ROI selected, b. Many of small holes detected on the irradiated ROI leads to non-uniform surface.

Table 1: Laser parameters considered for 3 mm and 5 mm BS with varies in *F*, PW and RR.

Sample number	Number of irradiation	BS (mm)	*F* (J/cm^2)	PW (ms)	RR (Hz)
1	10	3	210 - 300	100	1.0
2	10	3	210 - 300	200	1.0
3	10	3	210 - 300	300	1.0
4	10	3	210 - 300	100	1.5
5	10	3	210 - 300	200	1.5
6	10	3	210 - 300	300	1.5
7	10	3	210 - 300	100	2.0
8	10	3	210 - 300	200	2.0
9	10	3	210 - 300	300	2.0
10	10	5	150 - 240	100	1.0
11	10	5	150 - 240	200	1.0
12	10	5	150 - 240	300	1.0
13	10	5	150 - 240	100	1.5
14	10	5	150 - 240	200	1.5
15	10	5	150 - 240	300	1.5
16	10	5	60 - 150	100	2.0
17	10	5	60 - 150	200	2.0
18	10	5	60 - 150	300	2.0

Note: Maximum *F* for 3 mm BS is 300 J/cm^2 for all laser parameters. Meanwhile the maximum *F* for 5 mm BS is 240 J/cm^2 set-up with RR 1.0 and 1.5 Hz whereas 150 J/cm^2 set-up with RR 2.0 Hz.

Table 2: Summarize of ϵ for car coated substrate samples A1 – A18, B1 – B18 and C1 – C18.

Sample	*d* (μm)			*F* (J cm^{-2})			ϵ (μm cm^2 J^{-1})
	y_2	y_1	$dy = y_2 - y_1$	x_2	x_1	$dx = x_2 - x_1$	dy / dx
A1	90	67	23	300	210	90	0.26
A2	87	62	25	300	210	90	0.28
A3	112	65	47	300	210	90	0.52
A4	82.5	65.25	17.25	300	210	90	0.19
A5	98	84.25	13.75	300	210	90	0.15
A6	100	72	28	300	210	90	0.31
A7	112.5	73	39.5	300	210	90	0.44
A8	108.5	89	19.5	300	210	90	0.22
A9	123.5	92	31.5	300	210	90	0.35
A10	180	22.5	157.5	240	150	90	1.75
A11	130	75	55	240	150	90	0.61
A12	105	70	35	240	150	90	0.39
A13	120	88.5	31.5	240	150	90	0.35
A14	106	68.5	37.5	240	150	90	0.42
A15	97	72	25	240	150	90	0.28
A16	100	68	32	150	60	90	0.36
A17	125	71	54	150	60	90	0.60
A18	132.5	88	44.5	150	60	90	0.49
B1	230	182.5	47.5	300	210	90	0.53
B2	296.25	218.8	77.5	300	210	90	0.86
B3	212.5	168.8	43.75	300	210	90	0.49
B4	196	165	31	300	210	90	0.34
B5	255	158.5	96.5	300	210	90	1.07
B6	218	161	57	300	210	90	0.63
B7	195	160	35	300	210	90	0.39
B8	460	15	445	300	210	90	4.94
B9	385	295	90	300	210	90	1.00
B10	211.3	157.5	53.8	240	150	90	0.60
B11	275	173.8	101.2	240	150	90	1.12
B12	211.3	162.5	48.8	240	150	90	0.54
B13	213	155	58	240	150	90	0.64
B14	207	136	71	240	150	90	0.79
B15	224	162	62	240	150	90	0.69
B16	178.5	105	73.5	150	60	90	0.82
B17	183	121.5	61.5	150	60	90	0.68
B18	193.5	150.5	43	150	60	90	0.48
C1	235	163.8	71.25	300	210	90	0.79
C2	197.5	167.5	30	300	210	90	0.33
C3	220	165	55	300	210	90	0.61
C4	205	161	44	300	210	90	0.49
C5	211.5	184	27.5	300	210	90	0.31
C6	196	154	42	300	210	90	0.47
C7	207.5	169.5	38	300	210	90	0.42
C8	199	177	22	300	210	90	0.24
C9	221	175	46	300	210	90	0.51
C10	218.75	157.5	61.25	240	150	90	0.68

C11	210	115	95	240	150	90	1.06
C12	213.75	105	108.75	240	150	90	1.21
C13	223.75	142.5	81.25	240	150	90	0.90
C14	221.25	195	26.25	240	150	90	0.29
C15	228.75	127.5	101.25	240	150	90	1.13
C16	202.5	53.75	148.75	150	60	90	1.65
C17	196.25	57.5	138.75	150	60	90	1.54
C18	193.75	65	128.75	150	60	90	1.43

Table 3: Selected best crater depth from highest ϵ of substrate samples A, B and C.

Substrate sample	Selected substrate sample	Selected crater depth
A	A 10	Number 7
B	B 11	Number 3
C	C 16	Number 1

Table 4: Elemental composition by at. % and wt. % of each element indentified for PW 100 ms, RR 1.0 Hz, BS 5 mm and fluence energy 180 J/cm^2 for sample A10; Ten elements detected on the ROI selected at 10 kV of EDX system including Mg, Na and Ni.

Sample	Element	at. %	wt. %	wt. sigma %
A10	C	33.65	17.78	1.34
	O	37.13	26.12	1.51
	Na	2.05	2.08	0.58
	Mg	0.62	0.66	0.2
	Al	2.52	2.99	0.31
	Si	2.61	3.23	0.33
	P	6.87	9.36	0.68
	Ti	3.84	8.08	0.95
	Ni	3.63	9.36	4.38
	Zn	7.08	20.34	1.36
	Total:	100	100	-

Table 5: Elemental composition by at. % and wt. % of each element indentified for PW 200 ms, RR 1.0 Hz, BS 5 mm and fluence energy 220 J/cm^2 for sample B11; Nine elements detected on the ROI selected at 10 kV of EDX system including Na, Al and Ti.

Sample	Element	at. %	wt. %	wt. sigma %
B11	C	44.62	25.66	0.96
	O	32.76	25.09	0.83
	Na	1.41	1.55	0.41
	Al	0.34	0.45	0.16
	Si	0.82	1.11	0.18
	P	6.39	9.48	0.46
	Ti	5.42	12.43	0.8
	Fe	3.31	8.85	1.62

	Zn	4.92	15.4	0.75
	Total:	100	100	-

Table 6: Elemental composition by at. % and wt. % of each element indentified for PW 100 ms, RR 2.0 Hz, BS 5 mm and fluence energy 150 J/cm^2 for sample C16; Ten elements detected on the ROI selected at 10 kV of EDX system including Na, Si and S.

Sample	Element	at. %	wt. %	wt. sigma %
C16	C	44.43	23.07	0.82
	O	31.79	21.99	0.65
	Na	3.21	3.19	0.53
	Si	0.47	0.57	0.14
	P	4.86	6.5	0.31
	S	0.42	0.58	0.16
	Cr	0.9	2.01	0.56
	Fe	0.91	2.19	1.16
	Zn	12.03	34	0.93
	Ba	0.99	5.88	1.04
	Total:	100	100	-

Table 7: Elemental composition by at. % and wt. % of each element indentified for non-irradiated of sample A, B and C; Seven elements detected on the ROI selected at 10 kV of EDX system including C and O.

Elements	Background A			Background B			Background C		
	at. %	wt. %	wt. sigma %	at. %	wt. %	wt. sigma %	at. %	wt. %	wt. sigma %
C	65.63	58.22	2.41	80.55	73.69	0.84	37.63	20.52	0.86
O	18.57	21.95	1.45	18.11	22.06	0.75	38.93	28.28	0.86
N	14.4	14.9	3.08	-	-	-	12.52	37.15	1.22
Ti	1.4	4.94	0.91	0.9	3.28	0.56	-	-	-
Si	-	-	-	0.45	0.96	0.17	-	-	-
Na	-	-	-	-	-	-	3.61	3.77	0.82
P	-	-	-	-	-	-	7.31	10.28	0.8
Total	100	100	-	100	100	-	100	100	-

APPENDIX 1


(1). 240 J/cm^2

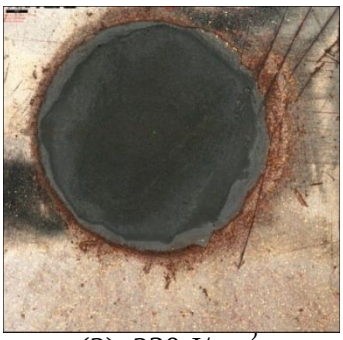
(2). 230 J/cm^2

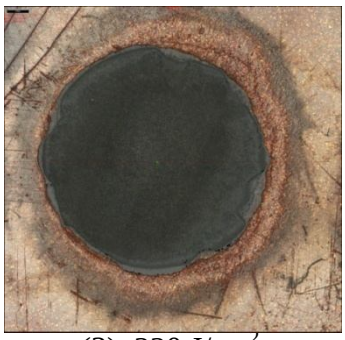
(3). 220 J/cm^2

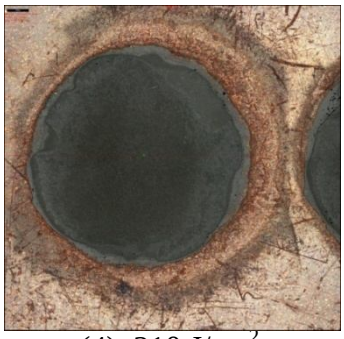
(4). 210 J/cm^2


(5). 200 J/cm^2


(6). 190 J/cm^2

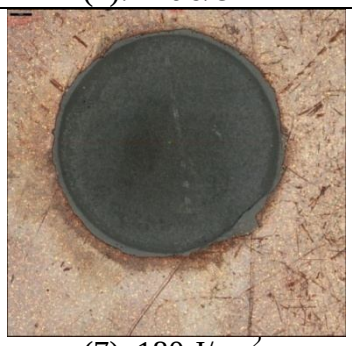
(7). 180 J/cm^2


(8). 170 J/cm^2

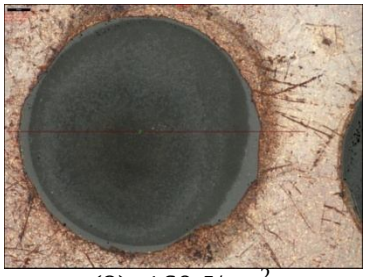
(9). 160 J/cm^2

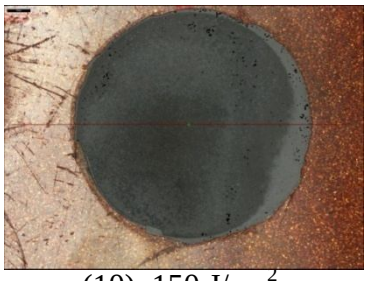
(10). 150 J/cm^2

A.1: IFM images represent the crater surface morphology for sample A10 with laser parameters fixed for beam size 5 mm, repetition rate 1.0 Hz and pulse width 100 ms.

APPENDIX 2

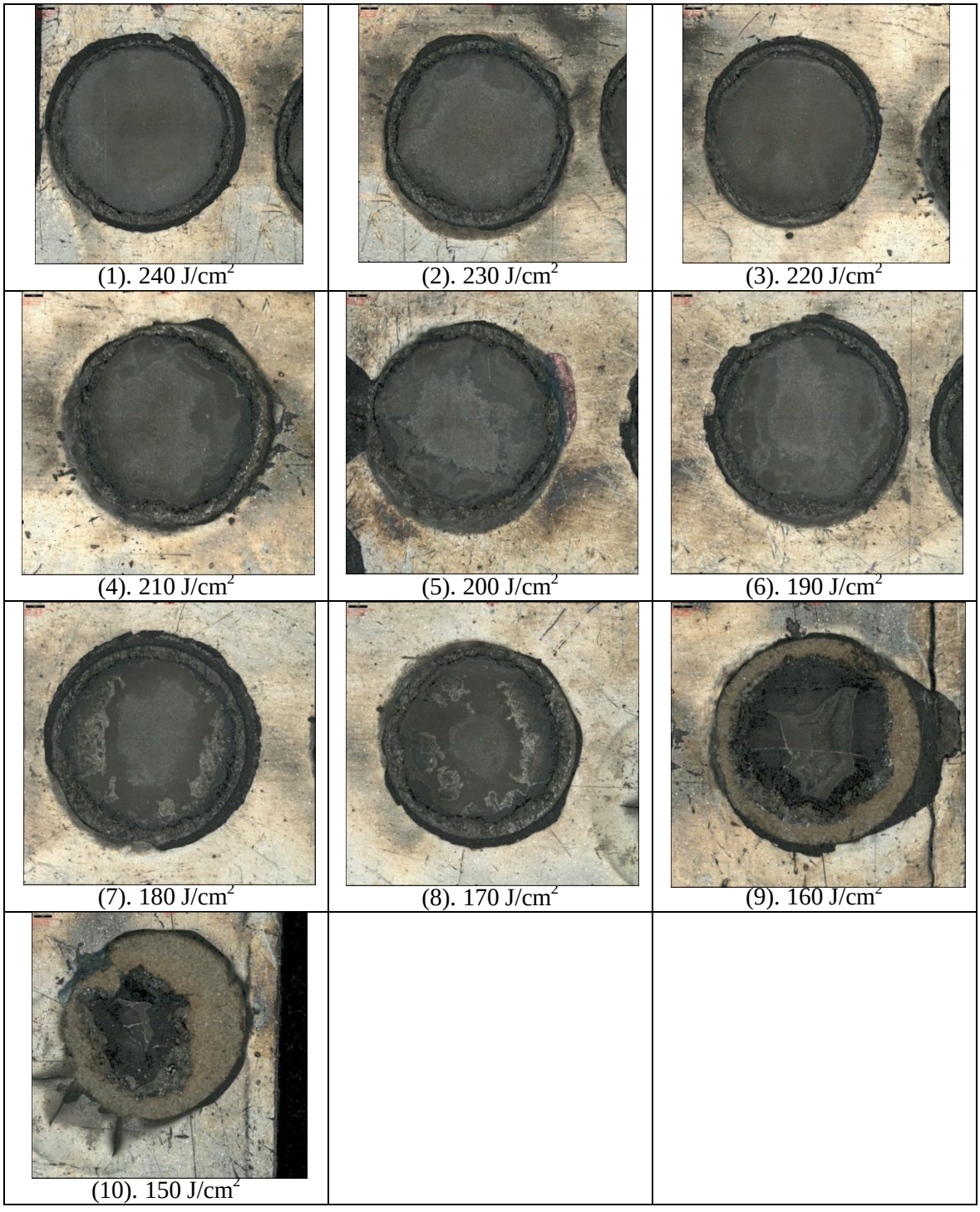

A.2: IFM images represent the crater surface morphology for sample B11 with laser parameters fixed for beam size 5 mm, repetition rate 1.0 Hz and pulse width 200 ms.

APPENDIX 3


(1). 150 J/cm^2

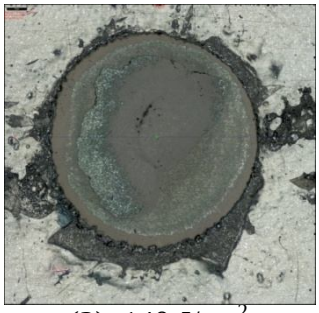
(2). 140 J/cm^2

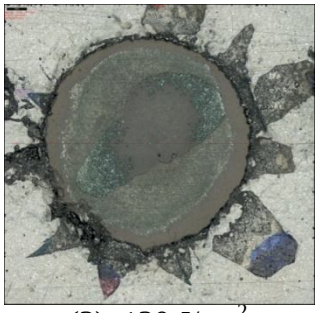
(3). 130 J/cm^2

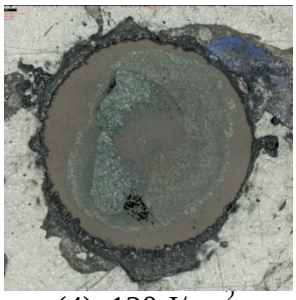
(4). 120 J/cm^2


(5). 110 J/cm^2

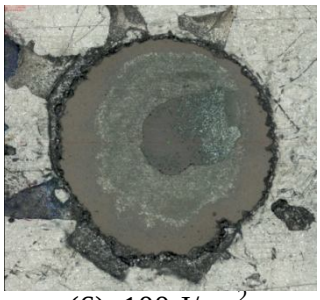
(6). 100 J/cm^2

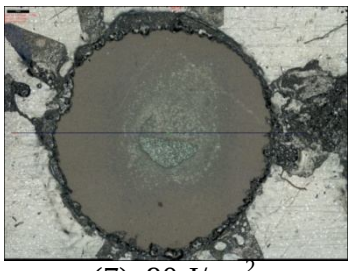
(7). 90 J/cm^2

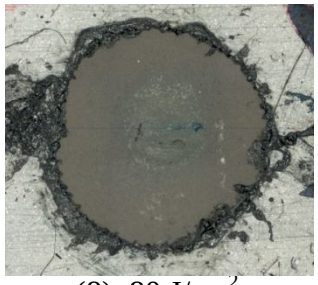
(8). 80 J/cm^2

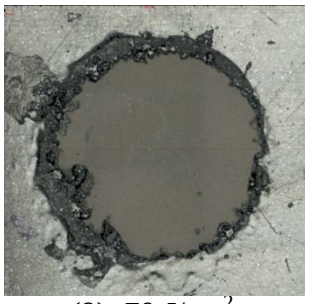
(9). 70 J/cm^2

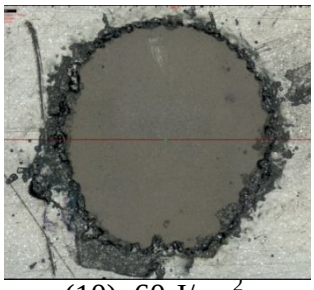
(10). 60 J/cm^2

A.3: IFM images represent the crater surface morphology for sample C16 with laser parameters fixed for beam size 5 mm, repetition rate 2.0 Hz and pulse width 100 ms.